A Case Study of Spectral Signature Detection in Multimodal and Outlier-Contaminated Scenes

David R. Thompson, Lukas Mandrake, Robert O. Green, Steve A. Chien

Abstract—**Mapping localized spectral features in complex scenes demands sensitive and robust detection algorithms. This work investigates two aspects of large images that can harm Matched Filter (MF) detection performance. First,** *multimodal backgrounds* **may violate normality assumptions. Second,** *outlier features* **can trigger false detections due to large projections onto the target vector. We review two state of the art methods designed to resolve these issues. The background clustering of Funk et al. [1] models multimodal backgrounds, and the Mixture Tuned Matched Filter (MT-MF) of Boardman and Kruse [2] addresses outliers. We demonstrate that combining the two methods has additional performance benefits. A Mixture Tuned Cluster Matched Filter (MT-CMF) shows effective performance on simulated and airborne datasets. We demonstrate target detection scenarios that evidence multimodality, outliers, and their combination. These experiments explore performance of the component algorithms and the practical circumstances that can favor a combined approach.**

I. INTRODUCTION

Imaging spectrometers can play an important role in both Earth Science [3] and planetary geology [4]. The spatial resolution, spectral resolution and sensitivity of these instruments continues to improve, enabling ever-subtler discrimination of minerals [5] species [6], [7], and synthetics [8]. The ability to combine morphological cues with compositional detail gives them important role in solar system exploration [4]. Detection of subtle spatially localized signals is a common challenge across all of these domains. Such signals commonly appear as subpixel fractions against a background substrate, and are difficult to identify reliably. Subpixel detection is related to the challenges of spectrometer mapping [9], classification [10], and abundance estimation [11]. Here we consider the challenge of detecting a specific anticipated target at subpixel abundances. We will assume that its spectral properties are known from prior in-situ or laboratory measurement.

The Matched Filter (MF) is the classical strategy for weak signal detection in such cases [12]. It models a d-dimensional spectral signal $\mathbf{x}$ as a linear combination of a background distribution with the target $\mathbf{t}$. The filter is a d-vector $\mathbf{f}$ whose inner product $\mathbf{f}^T\mathbf{x}$ best discriminates the subpixel signal from the background. Assuming a target mixing fraction ϕ, a background having mean μ^* and covariance matrix Σ^*, and ignoring independent additive measurement noise, the measured spectrum can be written as a perturbed multivariate

contact: *David R. Thompson@jpl.nasa.gov*
Jet Propulsion Laboratory, California Institute of Technology, 4800 Oak Grove Drive, Pasadena CA, 91109 USA

normal distribution:

$$\mathbf{x} = (1 - \phi)N(\mu^*, \Sigma^*) + \phi\mathbf{t} \tag{1}$$

Matched Filter implementations often estimate background means and covariances from the data [12], [13]. For collected data $X = \{\mathbf{x}_i\}_{i=1}^n$ the sample estimates μ and Σ are:

$$\mu = \frac{1}{n}\sum_{\mathbf{x}_i \in X}\mathbf{x}_i \qquad \Sigma = \frac{1}{n}\sum_{\mathbf{x}_i \in X}(\mathbf{x}_i - \mu)(\mathbf{x}_i - \mu)^T \tag{2}$$

The optimal Matched Filter (MF) is the best linear projection to separate the distributions in which the target is present and absent. These differ only by a constant factor, having equivalent covariance statistics. The MF is defined as:

$$\alpha_i = \mathbf{f}^T\mathbf{x}_i \quad \text{for} \quad \mathbf{f} = \frac{\Sigma^{-1}\mathbf{t}}{\mathbf{t}^T\Sigma^{-1}\mathbf{t}} \tag{3}$$

The expected MF score α is the mixing ratio ϕ, which ranges from zero to one.

MF detection is a broad and active area of remote sensing research, and there are many other formulations. Variants such as Adaptive Subspace Detectors [14] can improve performance by exploiting information about the target distribution. The Finite Target Matched Filter [15] further estimates the mixing fraction with Maximum Likelihood and uses the optimal likelihood ratio test for detection. We also note recent nonlinear matched filters based on kernel techniques [16]. We refer the interested reader to extensive taxonomies by Manolakis et al. and Kraut et al [14], [17], [18].

This paper investigates the general problem of robust MF detection for challenging background distributions. Several assumptions of the traditional Matched Filter are difficult to satisfy for large, complex scenes [19], [20]. First we consider the problem of *multimodal backgrounds*. Realistic backgrounds are seldom normally distributed. Neglecting intimate mixing, measured reflectances are convex combinations of component materials mixed in proportion to geographic area [11]. Scenes may also contain discrete terrain regions and geographic trends, resulting in data that is distributed along low-dimensional manifolds or split into clusters [1].

Outliers are another challenge. These small regions are caused by anomalous objects, glint, or instrument artifacts. It is difficult to characterize their statistical properties; they are numerically distinctive and may not significantly affect the sample covariance. However, their projection onto the MF vector may still have high magnitude [2]. Outliers therefore have high propensity to cause false alarms, and are generally not feasible convex combinations of the background and target.

Here we review two illustrative techniques that address

each of these scenarios and show that their combination has significant additional performance benefits. We use the background clustering of Funk et al. [1] to model multimodal backgrounds, and apply the Mixture Tuned Matched Filter (MT-MF) of Boardman et al. to mitigate outliers [2]. The combined Mixture Tuned Cluster Matched Filter (MT-CMF) shows promising performance on simulated and airborne datasets. Tests demonstrate practical target detection and mapping scenarios that evidence multimodality, outliers, and both effects in combination. These experiments show the success and failure modes for each component algorithm, and the circumstances that would favor a combined approach.

II. APPROACH

A. Preconditioning

We will assume the spectral data has been atmospherically corrected and transformed to reflectance. A preprocessing step known as the Minimum Noise Fraction transform (MNF) whitens the data to have zero mean and uncorrelated unit noise [2]. Methods for estimating noise properties include calibrating with dark images or empirical estimation from the scene [21], [22]. We use the empirical method of [2]. This assumes the background is locally homogeneous, so that differences between neighboring pixels are due to measurement noise. It estimates the covariance of this noise using the difference between each image pixel $\mathbf{x}_i$ and the set of two neighbors to the east and south, denoted $Q_{\mathbf{x}_i}$. We average these contributions, dividing by 1.5 to account for both terms as in [2]. The noise covariance then decomposes via Singular Value Decomposition into orthogonal matrices $\mathbf{U}_N$ and $\mathbf{V}_N$, and diagonal eigenvalue matrix $\mathbf{D}_N$.

$$\mathbf{U}_N \mathbf{D}_N \mathbf{V}_N^T = \frac{1}{1.5\,(n-1)} \sum_{\mathbf{x}_i \in X} \sum_{\mathbf{x}_j \in Q_{\mathbf{x}_i}} (\mathbf{x}_i - \mathbf{x}_j)(\mathbf{x}_i - \mathbf{x}_j)^T \tag{4}$$

We calculate each zero-mean noise-whitened datapoint $\mathbf{x}_i'$ by projection onto the principal components, with a magnitude that makes the noise distribution unit-variance isotropic.

$$\mathbf{x}_i' = \mathbf{D}_N^{-1/2} \mathbf{U}_N (\mathbf{x}_i - \hat{\mu}) \tag{5}$$

The MNF transform then performs a second singular value decomposition and rotation onto the principal components. The result is that datapoints have a convenient zero mean representation, with orthogonal channels ordered by eigenvalue.

$$\mathbf{U}\mathbf{D}\mathbf{V}^T = \frac{1}{n} \sum_{\mathbf{x}_i \in X} \mathbf{x}_i \mathbf{x}_i^T \tag{6}$$

$$\mathbf{x}'' = \mathbf{U}\mathbf{x}' \tag{7}$$

This preprocessing is implicit in all the analyses that follow, so we will drop primes from our notation. We also apply the same transformation to all target spectra before detection.

B. Background Clustering

MF target detection assumes that the background is Gaussian. Most implementations compute background covariance using a local fixed size window [12], [20]. This rectangular

region is arbitrary and its data may not actually be Gaussian-distributed. In contrast, the background clustering method of Funk et al. [1] seeks backgrounds that are compact and Gaussian, but not necessarily contiguous. A k-means clustering algorithm partitions the data into k disjoint background sets $\{M_j\}_{j=1}^k$, each with a sample mean μ_j and covariance matrix Σ_j. The resulting backgrounds are more compact and easier to separate from the target signal. We will refer to this technique as the Cluster Matched Filter (CMF).

The k-means clustering algorithm seeks cluster memberships that minimize inter-cluster variance [23]. Cluster centroids begin initialized to random data points. An *assignment* step assigns each data point to the closest centroid. Then, an *update* sets each centroid to be the mean of its member data points. This continues until convergence, which rarely requires more than a few iterations. High-dimensional data requires special care; spectral channels in the original representation are highly correlated, and Euclidean distance may not be physically meaningful. Funk et al. favor a distance metric that reflects the covariance of the spectral bands. Our MNF rotation provides this already, thanks to its principal component representation. We perform clustering using the three most significant MNF channels. Performance is generally insensitive to the number of channels retained.

To analyze a candidate spectrum the CMF identifies the nearest cluster centroid $j = \arg\min_j \|\mu_j - \mathbf{x}_i\|_2$. It uses the corresponding matched filter $\mathbf{f}_j$ given by:

$$\alpha_i = \mathbf{f}_j^T (\mathbf{x}_i - \mu_j) = \left[\frac{\Sigma_j^{-1}\mathbf{t}}{\mathbf{t}^T \Sigma_j^{-1} \mathbf{t}} \right]^T (\mathbf{x}_i - \mu_j) \tag{8}$$

If backgrounds are multimodal or distributed along manifolds, the local covariance provides a more accurate probability density and improves target/background separation.

C. Mixture Tuned Matched Filtering

The Mixture Tuned Matched Filter (MT-MF) of Boardman et al. is a partial unmixing approach combining MF detection with outlier rejection [2]. It augments the MF score with a second value β_i representing mixing feasibility, the probability of the observation assuming it is a convex combination of the background and the target. This penalizes points with a large magnitude perpendicular to the MF, discriminating feasible mixtures from statistical anomalies that are improbable under Equation 1. The MT-MF typifies other methods that use a decision boundary in a two dimensional space, such as the false alarm mitigation of DiPietro et al. [24].

The MT-MF estimates the mixing fraction with $\alpha_i = \mathbf{f}^T \mathbf{x}_i$ and background contribution $\mathbf{x}_i - \alpha_i \mathbf{t}$. It estimates the likelihood of this signal with respect to the known background distribution, an operation simplified by the MNF transform due to isotropy and unit noise. It is sufficient to use the L2 norm of the result, adjusting channels by the square root of the MNF eigenvalues and unit noise. This yields the mixture tuning vector $\mathbf{q}_i$. For each channel l, we have:

$$\mathbf{q}_i(l) = \frac{\mathbf{x}_i(l) - \alpha_i \mathbf{t}(l)}{\mathbf{D}(l)^{1/2}(1 - \alpha_i) - 1} \tag{9}$$

The mixing feasibility is $\beta_i = \|\mathbf{q}_i\|_2$. Together, the mixing feasibility β_i and matched filter response α_i tell whether the point is anomalous, and a good match to the target, respectively. Here we use the quantity α_i/β_i as a detection score, which offers consistent performance across all datasets. This expression resembles the Adaptive Coherence Estimator [25], though in principle the MT-MF detection statistic can be any monotonic function of α and β.

D. The Mixture Tuned Cluster Matched Filter

Our proposed approach combines background clustering with mixture feasibility. We apply the MNF transform followed by k-means clustering. We then estimate each cluster's mean, covariance, and the corresponding eigenvalues. This yields a cluster-specific MF estimate α_i but also a cluster-specific feasibility score β_i (Algorithm 1 below).

Input: Image $\{\mathbf{x}_i\}_{i=1}^n$, number clusters k, target $\mathbf{t}$
Output: Matched filter indices $\{\alpha_i, \beta_i\}_{i=1}^n$

Compute data mean $\hat{\mu} = \frac{1}{n}\sum_{\mathbf{x}_i \in X}(\mathbf{x}_i)$;
Apply MNF transform using Equation 7;
Find clusters $\{M_j\}_{j=1}^k$ with k-means;
Compute cluster means $\{\mu_j\}_{j=1}^k$, covariances $\{\Sigma_j\}_{j=1}^k$ **foreach**
cluster M_j **do**
    Singular Value Decomposition: $\Sigma_j = \mathbf{U}_j \mathbf{D}_j \mathbf{V}_j^T$;
    Compute Cluster Matched Filter $\mathbf{f}_j = \hat{\Sigma}_j^{-1}\mathbf{t}/(\mathbf{t}^T\hat{\Sigma}_j^{-1}\mathbf{t})$;
    foreach $\mathbf{x}_i \in M_j$ **do**
        $\mathbf{x}_i \leftarrow U_j(\mathbf{x}_i - \mu_j)$;
        $\alpha_i = \mathbf{f}_j^T \mathbf{x}_i$;
        foreach l **do**
            $\mathbf{q}_i(l) = \frac{\mathbf{x}_i(l) - \alpha_i \mathbf{t}(l)}{\mathbf{D}_j(l)^{1/2}(1-\alpha_i)^{-1}}$;
        end
        $\beta_i = \|\mathbf{q}\|_2$;
    end
end

Algorithm 1: Mixture Tuned Cluster Matched Filter

A simple "Daisyworld" simulation [1] demonstrates its performance. We generate a simple size 1000 dataset drawn from two Gaussian distributions having opposite correlation coefficients. We simulate outliers by optionally drawing 33% of the population from a much broader Gaussian distribution (Figure 1). A series of tests evaluate MF, CMF, MT-MF, and MT-CMF strategies by generating random target signatures uniformly distributed throughout the range of actual (non-outlier) background data. We inject this target at a 10% mixing fraction into each background spectrum.

We perform 100 trials for each of three scenarios: a multimodal scenario with two Gaussians, a unimodal background with outliers, and a multimodal background with outliers. For each trial we compute the fraction of true positives achieved at a constant 1% false alarm rate. Figure 2 shows the resulting scores expressed as percentiles. The original MF never outperforms any of the variants. The CMF performs well if its assumptions are satisfied, but is sensitive to outliers. Conversely the MT-MF method is robust in the presence of outliers, but its performance is reduced for the multimodal background. The MT-CMF outperforms the other methods with an increasing margin as task difficulty increases.
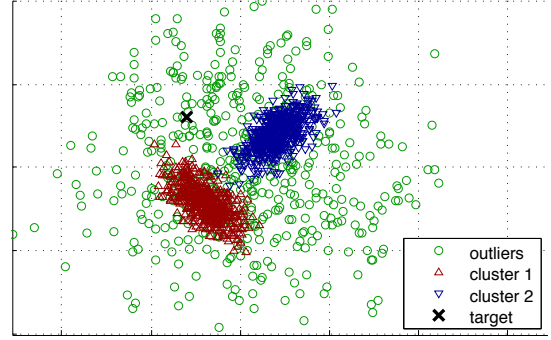

Fig. 1. Daisyworld simulation, as in Funk et al. [1]. We generate data from either one or two clusters, as well as a much broader "outlier" distribution.
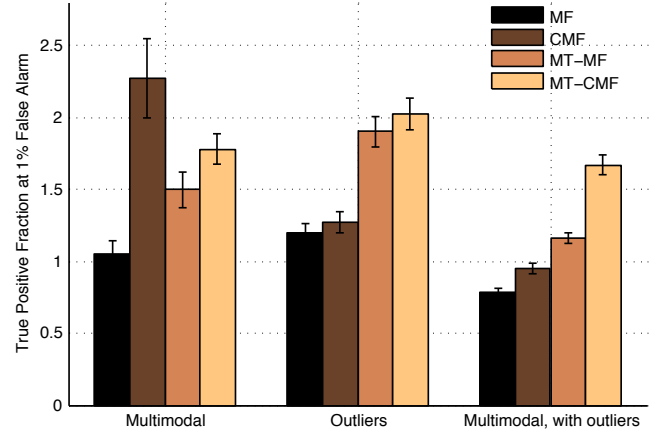

Fig. 2. Fraction of actual targets detected at a 1% false alarm rate for the daisyworld simulation.
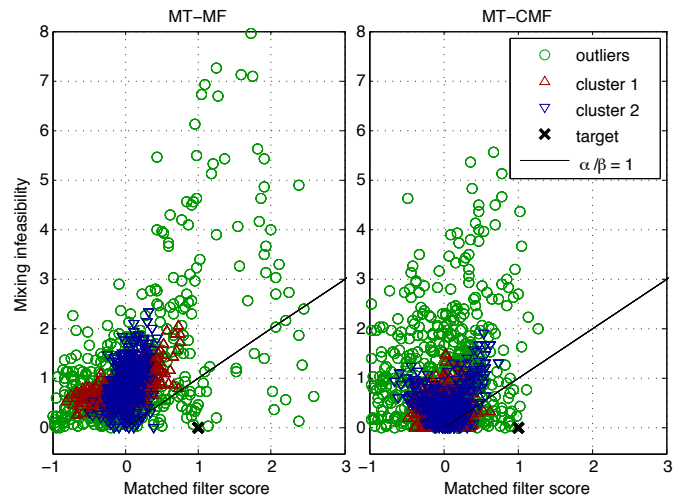

Fig. 3. MT-MF and MT-CMF scores for the daisyworld simulation. We plot points according to generating distribution (rather than the MT-CMF estimate of cluster memberships). The black 'x' indicates the location of the target, and the black line shows an isocontour of constant α/β. The MT-CMF reduces spurious false alarms with high incidental MF scores.
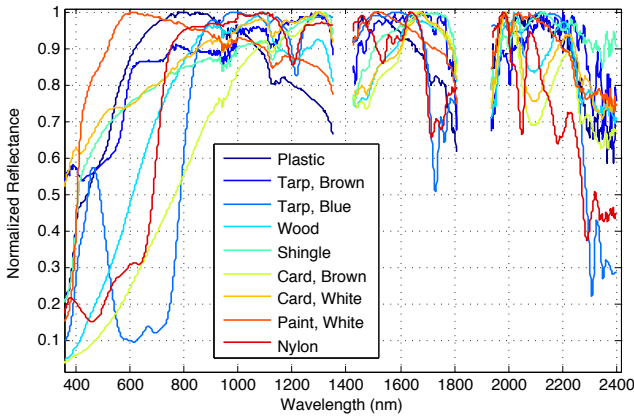
Fig. 5. Target signatures used in simulations.

Figure 3 illustrates this phenomenon visually. It shows matched filter scores α and mixing feasibility β using MT-MF and MT-CMF methods, with points labeled according to generating distribution. The MT-CMF estimates α and β independently for each background cluster which results in more compact distributions. The target lies on the border between these two clusters, and an accruate multimodal background is necessary to detect it reliably.

III. Evaluation

We evaluate the algorithms for a physical remote sensing scenario by introducing simulated targets into reflectance data from an airborne instrument. AVIRIS, the Airborne Visible Infrared Imaging Spectrometer (AVIRIS) [3], [26], is an imager carried onboard ER-2 and Twin Otter turboprop platforms. It acquires spectra in the 400-2500nm range with 10nm spectral resolution. We use a subset of data from a Twin Otter flightline over desert terrain in which the images have a spatial resolution of approximately 3m. We select three 256×256 image tiles representing diverse natural and artificial environments (Figure 4). The *mountain pass* is comprised of open terrain with several subtle terrain variations. A *golf course* scene introduces localized outlier features. Finally an urban *casino* scene is the most complex, containing a wide range of artificial materials, terrain, and large buildings. The AVIRIS radiance data was atmospherically corrected and transformed to reflectance.

We acquired target spectra from physical samples representing a range of natural and synthetic materials. These include blue and brown nylon tarps, synthetic brown and white card, white paint, treated nylon fabric, and raw building materials such as unstained wood, molded plastic, and roofing shingles. We acquired these reflectance spectra manually under direct sunlight using an ASD field spectrometer having 10nm spectral resolution throughout the 350-2400nm range. Figure 5 shows the resulting target spectra after normalizing by the maximum value.

In order to meaningfully compare algorithms we create a challenging task by intentionally injecting target signals at a fractional fill level near the detection limit. We introduce each target at a 1% fractional fill, equivalent to a square 30 cm wide.

Our test data combines these targets into the reflectance data with compensatory scaling to account for the area "covered" by the virtual target.

IV. Results and Discussion

Our performance evaluation compares the resulting detection statistics against the background pixels. We found that performance of the cluster-based algorithms insensitive to the number of clusters used; here we set k=10 for all images and clustering methods. Table IV reports the true positive fraction at a constant false alarm rate of 0.1%. The top-scoring method for each scenario appears in bold.

The results largely corroborate the simplified Daisyworld simulation. The classical MF performs worst. Both Mixture Tuned and Cluster Matched Filters outperform each other for different background/target combinations. The CMF excels for the mountain pass scene with few outliers but subtle surface variations. In contrast, the MT-MF offers superior outlier rejection for the homogeneous background of the golf course. Overall, the combined algorithm performs best in each scenario. Often it is able to achieve significantly better detection rates than either component technique independently. This is particularly true for the most challenging scene, which combines scattered outliers with multimodality.

TABLE I
TRUE POSITIVE FRACTION DETECTED AT A 0.1% FALSE ALARM RATE.

Mountain Pass			
Target	MF	CMF	MT-MF	MT-CMF
1. Plastic	0.75	**1.00**	0.92	**1.00**
2. Tarp, Brown	0.99	**1.00**	0.99	**1.00**
3. Tarp, Blue	**1.00**	**1.00**	**1.00**	**1.00**
4. Wood	0.65	**1.00**	0.86	**1.00**
5. Shingle	0.98	**1.00**	0.99	**1.00**
6. Card, Brown	0.43	**1.00**	0.70	**1.00**
7. Card, White	0.87	**1.00**	0.97	**1.00**
8. Paint, White	0.85	**1.00**	0.95	**1.00**
9. Nylon	0.99	**1.00**	0.99	**1.00**

Golf Course			
Target	MF	CMF	MT-MF	MT-CMF
1. Plastic	**1.00**	0.96	**1.00**	**1.00**
2. Tarp, Brown	**1.00**	**1.00**	**1.00**	**1.00**
3. Tarp, Blue	0.97	**1.00**	0.99	**1.00**
4. Wood	**1.00**	0.96	**1.00**	**1.00**
5. Shingle	**1.00**	**1.00**	**1.00**	**1.00**
6. Card, Brown	0.96	0.93	**0.98**	**0.98**
7. Card, White	**1.00**	0.97	**1.00**	**1.00**
8. Paint, White	**1.00**	0.97	**1.00**	**1.00**
9. Nylon	0.95	0.99	0.98	**1.00**

Casino / Highway			
Target	MF	CMF	MT-MF	MT-CMF
1. Plastic	0.03	0.46	0.31	**0.55**
2. Tarp, Brown	0.85	0.94	0.87	**0.97**
3. Tarp, Blue	0.01	0.37	0.22	**0.60**
4. Wood	0.06	0.48	0.33	**0.59**
5. Shingle	0.89	0.96	0.87	**0.97**
6. Card, Brown	0.24	0.39	0.37	**0.53**
7. Card, White	0.40	0.72	0.66	**0.88**
8. Paint, White	0.20	0.60	0.55	**0.79**
9. Nylon	0.43	0.72	0.75	**0.92**

These results suggest that clustering might improve other MF variants. Candidates include the Finite Target Matched
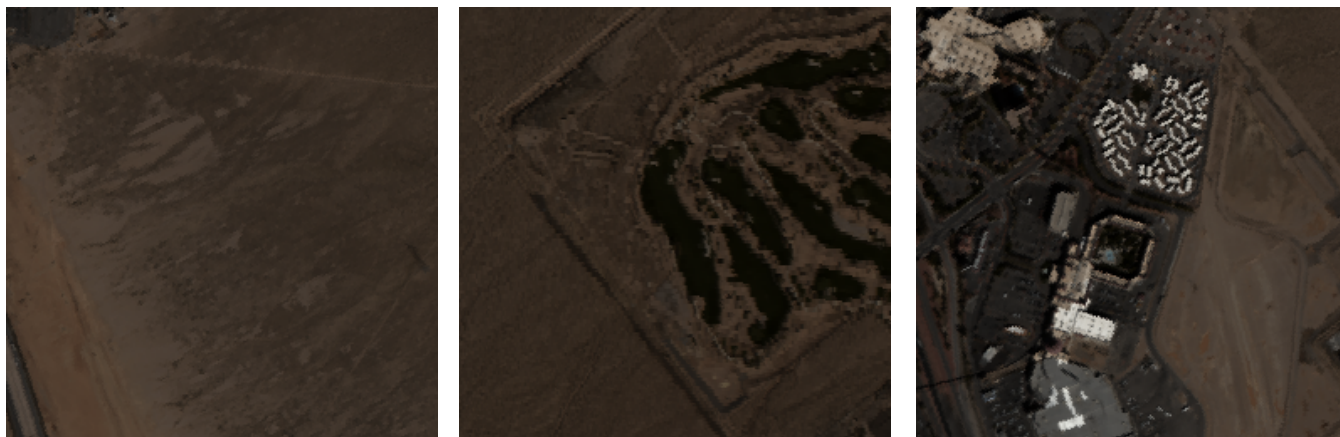
Fig. 4. Mountain Pass, Golf Course, and Casino AVIRIS scenes used in simulations (R:579nm, G:531nm, B:482nm).

Filter that estimates the Maximum Likelihood mixing fraction [15], and Adaptive Subspace Detectors that measure signal energy in the subspace of the target [14]. These typically rely on unimodal background assumptions, and might glean similar benefits from background clustering. Another promising avenue for further investigation would be to improve the background clustering technique. Robust estimation strategies might improve reliability for fitting multimodal background distributions to very noisy data. Regardless, the MT-CMF approach presented here is a good compromise. Simple implementation and robust performance make it a compelling option for Matched Filter detection in complex scenes.

REFERENCES

[1] C. C. Funk, J. Theiler, D. A. Roberts, and C. C. Borel, "Clustering to improve matched filter detection of weak gas plumes in hyperspectral thermal imagery," *TGARS*, vol. 39, no. 7, pp. 1410–1420, 2001.

[2] J. W. Boardman and F. A. Kruse, "Analysis of imaging spectrometer data using N-dimensional geometry and a mixture-tuned matched filtering (MTMF) approach," *TGARS*, vol. 49, no. 11, pp. 4138–4152, 2011.

[3] R. Green, "AVIRIS and related 21st century imaging spectrometers for Earth and space science," *High Performance Computing in Remote Sensing*, p. 335, 2008.

[4] B. Ehlmann, J. Mustard, S. Murchie, F. Poulet, J. Bishop *et al.*, "Orbital identification of carbonate-bearing rocks on Mars," *Science*, vol. 322, no. 5909, p. 1828, 2008.

[5] F. A. Kruse, J. W. Boardman, and J. F. Huntington, "Comparison of airborne hyperspectral data and EO-1 Hyperion for mineral mapping," *TGARS*, vol. 41, pp. 1388–1400, 2003.

[6] M. Clark, D. Roberts, and D. Clark, "Hyperspectral discrimination of tropical rain forest tree species at leaf to crown scales," *Remote Sensing of Environment*, vol. 96, no. 3, pp. 375–398, 2005.

[7] S. Ustin, D. Roberts, J. Gamon, G. Asner, and R. Green, "Using imaging spectroscopy to study ecosystem processes and properties," *BioScience*, vol. 54, no. 6, pp. 523–534, 2004.

[8] M. Herold, M. Gardner, and D. Roberts, "Spectral resolution requirements for mapping urban areas," *TGARS*, vol. 41, no. 9, pp. 1907–1919, 2003.

[9] G. A. Swayze, "The hydrothermal and structural history of the cuprite mining district, southwestern nevada: An integrated geological and geophysical approach," *Ph.D. thesis, Univ. Colorado, Boulder, CO*, 1997.

[10] R. N. Clark, G. A. Swayze, K. E. Livo, R. F. Kokaly, S. J. Sutley, J. B. Dalton, R. R. McDougal, , and C. A. Gent, "Imaging spectroscopy: Earth and planetary remote sensing with the usgs tetracorder and expert systems," *Journal of Geophysical Research*, vol. 108(E12), 5131, 2003.

[11] N. Keshava and J. Mustard, "Spectral unmixing," *Signal Processing Magazine, IEEE*, vol. 19, no. 1, pp. 44–57, 2002.

[12] A. D. Stocker, I. S. Reed, and X. Yu, "Mu1tidimensiona1 signal processing for electro-optical target detection," *SPIE Signal And Data Processing of Small Targets*, 1990.

[13] S. Kraut, L. Scharf, and R. Butler, "The adaptive coherence estimator: a uniformly most-powerful-invariant adaptive detection statistic," *IEEE Trans. Signal Processing*, vol. 53, no. 2, pp. 427–438, 2005.

[14] S. Kraut, L. L. Scharf, and L. T. McWhorter, "Adaptive subspace detectors," *IEEE Trans. Signal Processing*, vol. 49, no. 1, 2001.

[15] A. Schaum and A. Stocker, "Spectrally selective target detection," *Proc. International Symposium on Spectral Sensing Research*, 1997.

[16] H. Kwon and N. Nasrabadi, "Kernel spectral matched filter for hyperspectral imagery," *International Journal of Computer Vision*, vol. 71, pp. 127–141, 2007, 10.1007/s11263-006-6689-3.

[17] D. M. Dimitris G. Manolakis, Christina Siracusa and G. A. Shaw, "Hyperspectral adaptive matched-filter detectors: practical performance comparison," *Proceedings of SPIE*, vol. 4381, no. 18, 2001.

[18] D. Manolakis and G. Shaw, "Detection algorithms for hyperspectral imaging applications," *IEEE Signal Processing Magazine*, vol. 19, no. 1, pp. 29 –43, jan 2002.

[19] M. Eismann, "Strategies for hyperspectral target detection in complex background environments," in *Aerospace Conference, 2006 IEEE*. IEEE, 2006, p. 10.

[20] M. Eismann, J. Meola, and A. Stocker, "Automated hyperspectral target detection and change detection from an airborne platform: Progress and challenges," in *IEEE International Geoscience and Remote Sensing Symposium (IGARSS)*. IEEE, 2010, pp. 4354–4357.

[21] B. Gao, "An operational method for estimating signal to noise ratios from data acquired with imaging spectrometers," *Remote Sensing of Environment*, vol. 43, no. 1, pp. 23–33, 1993.

[22] B. Zhu, X. Wang, L. Tang, and C. Li, "Review on methods for SNR estimation of optical remote sensing imagery," *Remote Sensing Technology and Application*, vol. 25, no. 2, pp. 303–309, 2010.

[23] C. M. Bishop, *Pattern Recognition and Machine Learning*. New York: Springer, 2006, iSBN:978-0-387-31073-2.

[24] R. DiPietro, D. Manolakis, R. Lockwood, T. Cooley, and J. Jacobson, "Performance evaluation of hyperspectral detection algorithms for sub-pixel objects," *Proc. SPIE*, vol. 7695, 2010.

[25] L. L. Scharf and L. T. McWhorter, "Adaptive matched subspace detectors and adaptive coherence estimators," *Proc. 30th Asilomar Conference on Signals, Systems, and Computers*, 1996.

[26] R. Green, M. Eastwood, C. Sarture, T. Chrien, M. Aronsson, B. Chippendale, J. Faust, B. Pavri, C. Chovit, M. Solis *et al.*, "Imaging spectroscopy and the airborne visible/infrared imaging spectrometer (AVIRIS)," *Remote Sensing of Environment*, vol. 65, no. 3, pp. 227–248, 1998.